Measurement of the $WZ \to \ell\nu\ell\ell$ cross section and limits on anomalous triple gauge couplings in $p\bar{p}$ collisions at $\sqrt{s} = 1.96$ TeV

V.M. Abazov,[35] B. Abbott,[73] M. Abolins,[62] B.S. Acharya,[29] M. Adams,[48] T. Adams,[46] G.D. Alexeev,[35] G. Alkhazov,[39] A. Alton[a],[61] G. Alverson,[60] G.A. Alves,[2] L.S. Ancu,[34] M. Aoki,[47] Y. Arnoud,[14] M. Arov,[57] A. Askew,[46] B. Åsman,[40] O. Atramentov,[65] C. Avila,[8] J. BackusMayes,[80] F. Badaud,[13] L. Bagby,[47] B. Baldin,[47] D.V. Bandurin,[46] S. Banerjee,[29] E. Barberis,[60] A.-F. Barfuss,[15] P. Baringer,[55] J. Barreto,[2] J.F. Bartlett,[47] U. Bassler,[18] S. Beale,[6] A. Bean,[55] M. Begalli,[3] M. Begel,[71] C. Belanger-Champagne,[40] L. Bellantoni,[47] J.A. Benitez,[62] S.B. Beri,[27] G. Bernardi,[17] R. Bernhard,[22] I. Bertram,[41] M. Besançon,[18] R. Beuselinck,[42] V.A. Bezzubov,[38] P.C. Bhat,[47] V. Bhatnagar,[27] G. Blazey,[49] S. Blessing,[46] K. Bloom,[64] A. Boehnlein,[47] D. Boline,[70] T.A. Bolton,[56] E.E. Boos,[37] G. Borissov,[41] T. Bose,[59] A. Brandt,[76] O. Brandt,[23] R. Brock,[62] G. Brooijmans,[68] A. Bross,[47] D. Brown,[19] X.B. Bu,[7] D. Buchholz,[50] M. Buehler,[79] V. Buescher,[24] V. Bunichev,[37] S. Burdin[b],[41] T.H. Burnett,[80] C.P. Buszello,[42] P. Calfayan,[25] B. Calpas,[15] S. Calvet,[16] E. Camacho-Pérez,[32] J. Cammin,[69] M.A. Carrasco-Lizarraga,[32] E. Carrera,[46] B.C.K. Casey,[47] H. Castilla-Valdez,[32] S. Chakrabarti,[70] D. Chakraborty,[49] K.M. Chan,[53] A. Chandra,[78] G. Chen,[55] S. Chevalier-Théry,[18] D.K. Cho,[75] S.W. Cho,[31] S. Choi,[31] B. Choudhary,[28] T. Christoudias,[42] S. Cihangir,[47] D. Claes,[64] J. Clutter,[55] M. Cooke,[47] W.E. Cooper,[47] M. Corcoran,[78] F. Couderc,[18] M.-C. Cousinou,[15] A. Croc,[18] D. Cutts,[75] M. Ćwiok,[30] A. Das,[44] G. Davies,[42] K. De,[76] S.J. de Jong,[34] E. De La Cruz-Burelo,[32] F. Déliot,[18] M. Demarteau,[47] R. Demina,[69] D. Denisov,[47] S.P. Denisov,[38] S. Desai,[47] K. DeVaughan,[64] H.T. Diehl,[47] M. Diesburg,[47] A. Dominguez,[64] T. Dorland,[80] A. Dubey,[28] L.V. Dudko,[37] D. Duggan,[65] A. Duperrin,[15] S. Dutt,[27] A. Dyshkant,[49] M. Eads,[64] D. Edmunds,[62] J. Ellison,[45] V.D. Elvira,[47] Y. Enari,[17] S. Eno,[58] H. Evans,[51] A. Evdokimov,[71] V.N. Evdokimov,[38] G. Facini,[60] A.V. Ferapontov,[75] T. Ferbel,[58,69] F. Fiedler,[24] F. Filthaut,[34] W. Fisher,[62] H.E. Fisk,[47] M. Fortner,[49] H. Fox,[41] S. Fuess,[47] T. Gadfort,[71] A. Garcia-Bellido,[69] V. Gavrilov,[36] P. Gay,[13] W. Geist,[19] W. Geng,[15,62] D. Gerbaudo,[66] C.E. Gerber,[48] Y. Gershtein,[65] D. Gillberg,[6] G. Ginther,[47,69] G. Golovanov,[35] A. Goussiou,[80] P.D. Grannis,[70] S. Greder,[19] H. Greenlee,[47] Z.D. Greenwood,[57] E.M. Gregores,[4] G. Grenier,[20] Ph. Gris,[13] J.-F. Grivaz,[16] A. Grohsjean,[18] S. Grünendahl,[47] M.W. Grünewald,[30] F. Guo,[70] J. Guo,[70] G. Gutierrez,[47] P. Gutierrez,[73] A. Haas[c],[68] P. Haefner,[25] S. Hagopian,[46] J. Haley,[60] L. Han,[7] K. Harder,[43] A. Harel,[69] J.M. Hauptman,[54] J. Hays,[42] T. Hebbeker,[21] D. Hedin,[49] A.P. Heinson,[45] U. Heintz,[75] C. Hensel,[23] I. Heredia-De La Cruz,[32] K. Herner,[61] G. Hesketh,[60] M.D. Hildreth,[53] R. Hirosky,[79] T. Hoang,[46] J.D. Hobbs,[70] B. Hoeneisen,[12] M. Hohlfeld,[24] S. Hossain,[73] Y. Hu,[70] Z. Hubacek,[10] N. Huske,[17] V. Hynek,[10] I. Iashvili,[67] R. Illingworth,[47] A.S. Ito,[47] S. Jabeen,[75] M. Jaffré,[16] S. Jain,[67] D. Jamin,[15] R. Jesik,[42] K. Johns,[44] M. Johnson,[47] D. Johnston,[64] A. Jonckheere,[47] P. Jonsson,[42] J. Joshi,[27] A. Juste[d],[47] K. Kaadze,[56] E. Kajfasz,[15] D. Karmanov,[37] P.A. Kasper,[47] I. Katsanos,[64] R. Kehoe,[77] S. Kermiche,[15] N. Khalatyan,[47] A. Khanov,[74] A. Kharchilava,[67] Y.N. Kharzheev,[35] D. Khatidze,[75] M.H. Kirby,[50] M. Kirsch,[21] J.M. Kohli,[27] A.V. Kozelov,[38] J. Kraus,[62] A. Kumar,[67] A. Kupco,[11] T. Kurča,[20] V.A. Kuzmin,[37] J. Kvita,[9] S. Lammers,[51] G. Landsberg,[75] P. Lebrun,[20] H.S. Lee,[31] W.M. Lee,[47] J. Lellouch,[17] L. Li,[45] Q.Z. Li,[47] S.M. Lietti,[5] J.K. Lim,[31] D. Lincoln,[47] J. Linnemann,[62] V.V. Lipaev,[38] R. Lipton,[47] Y. Liu,[7] Z. Liu,[6] A. Lobodenko,[39] M. Lokajicek,[11] P. Love,[41] H.J. Lubatti,[80] R. Luna-Garcia[e],[32] A.L. Lyon,[47] A.K.A. Maciel,[2] D. Mackin,[78] R. Madar,[18] R. Magaña-Villalba,[32] S. Malik,[64] V.L. Malyshev,[35] Y. Maravin,[56] J. Martínez-Ortega,[32] R. McCarthy,[70] C.L. McGivern,[55] M.M. Meijer,[34] A. Melnitchouk,[63] D. Menezes,[49] P.G. Mercadante,[4] M. Merkin,[37] A. Meyer,[21] J. Meyer,[23] N.K. Mondal,[29] T. Moulik,[55] G.S. Muanza,[15] M. Mulhearn,[79] E. Nagy,[15] M. Naimuddin,[28] M. Narain,[75] R. Nayyar,[28] H.A. Neal,[61] J.P. Negret,[8] P. Neustroev,[39] H. Nilsen,[22] S.F. Novaes,[5] T. Nunnemann,[25] G. Obrant,[39] D. Onoprienko,[56] J. Orduna,[32] N. Osman,[42] J. Osta,[53] G.J. Otero y Garzón,[1] M. Owen,[43] M. Padilla,[45] M. Pangilinan,[75] N. Parashar,[52] V. Parihar,[75] S.K. Park,[31] J. Parsons,[68] R. Partridge[c],[75] N. Parua,[51] A. Patwa,[71] B. Penning,[47] M. Perfilov,[37] K. Peters,[43] Y. Peters,[43] G. Petrillo,[69] P. Pétroff,[16] R. Piegaia,[1] J. Piper,[62] M.-A. Pleier,[71] P.L.M. Podesta-Lerma[f],[32] V.M. Podstavkov,[47] M.-E. Pol,[2] P. Polozov,[36] A.V. Popov,[38] M. Prewitt,[78] D. Price,[51] S. Protopopescu,[71] J. Qian,[61] A. Quadt,[23] B. Quinn,[63] M.S. Rangel,[16] K. Ranjan,[28] P.N. Ratoff,[41] I. Razumov,[38] P. Renkel,[77] P. Rich,[43] M. Rijssenbeek,[70] I. Ripp-Baudot,[19] F. Rizatdinova,[74] M. Rominsky,[47] C. Royon,[18] P. Rubinov,[47] R. Ruchti,[53] G. Safronov,[36] G. Sajot,[14] A. Sánchez-Hernández,[32] M.P. Sanders,[25] B. Sanghi,[47] A.S. Santos,[5] G. Savage,[47] L. Sawyer,[57] T. Scanlon,[42] D. Schaile,[25] R.D. Schamberger,[70] Y. Scheglov,[39] H. Schellman,[50] T. Schliephake,[26] S. Schlobohm,[80] C. Schwanenberger,[43] R. Schwienhorst,[62] J. Sekaric,[55]

H. Severini,[73] E. Shabalina,[23] V. Shary,[18] A.A. Shchukin,[38] R.K. Shivpuri,[28] V. Simak,[10] V. Sirotenko,[47] P. Skubic,[73] P. Slattery,[69] D. Smirnov,[53] G.R. Snow,[64] J. Snow,[72] S. Snyder,[71] S. Söldner-Rembold,[43] L. Sonnenschein,[21] A. Sopczak,[41] M. Sosebee,[76] K. Soustruznik,[9] B. Spurlock,[76] J. Stark,[14] V. Stolin,[36] D.A. Stoyanova,[38] E. Strauss,[70] M. Strauss,[73] R. Ströhmer,[25] D. Strom,[48] L. Stutte,[47] P. Svoisky,[34] M. Takahashi,[43] A. Tanasijczuk,[1] W. Taylor,[6] B. Tiller,[25] M. Titov,[18] V.V. Tokmenin,[35] D. Tsybychev,[70] B. Tuchming,[18] C. Tully,[66] P.M. Tuts,[68] R. Unalan,[62] L. Uvarov,[39] S. Uvarov,[39] S. Uzunyan,[49] R. Van Kooten,[51] W.M. van Leeuwen,[33] N. Varelas,[48] E.W. Varnes,[44] I.A. Vasilyev,[38] P. Verdier,[20] L.S. Vertogradov,[35] M. Verzocchi,[47] M. Vesterinen,[43] D. Vilanova,[18] P. Vint,[42] P. Vokac,[10] H.D. Wahl,[46] M.H.L.S. Wang,[69] J. Warchol,[53] G. Watts,[80] M. Wayne,[53] G. Weber,[24] M. Weber[g],[47] M. Wetstein,[58] A. White,[76] D. Wicke,[24] M.R.J. Williams,[41] G.W. Wilson,[55] S.J. Wimpenny,[45] M. Wobisch,[57] D.R. Wood,[60] T.R. Wyatt,[43] Y. Xie,[47] C. Xu,[61] S. Yacoob,[50] R. Yamada,[47] W.-C. Yang,[43] T. Yasuda,[47] Y.A. Yatsunenko,[35] Z. Ye,[47] H. Yin,[7] K. Yip,[71] H.D. Yoo,[75] S.W. Youn,[47] J. Yu,[76] S. Zelitch,[79] T. Zhao,[80] B. Zhou,[61] J. Zhu,[70] M. Zielinski,[69] D. Zieminska,[51] and L. Zivkovic[68]

(The D0 Collaboration*)

[1] *Universidad de Buenos Aires, Buenos Aires, Argentina*
[2] *LAFEX, Centro Brasileiro de Pesquisas Físicas, Rio de Janeiro, Brazil*
[3] *Universidade do Estado do Rio de Janeiro, Rio de Janeiro, Brazil*
[4] *Universidade Federal do ABC, Santo André, Brazil*
[5] *Instituto de Física Teórica, Universidade Estadual Paulista, São Paulo, Brazil*
[6] *Simon Fraser University, Vancouver, British Columbia, and York University, Toronto, Ontario, Canada*
[7] *University of Science and Technology of China, Hefei, People's Republic of China*
[8] *Universidad de los Andes, Bogotá, Colombia*
[9] *Charles University, Faculty of Mathematics and Physics, Center for Particle Physics, Prague, Czech Republic*
[10] *Czech Technical University in Prague, Prague, Czech Republic*
[11] *Center for Particle Physics, Institute of Physics, Academy of Sciences of the Czech Republic, Prague, Czech Republic*
[12] *Universidad San Francisco de Quito, Quito, Ecuador*
[13] *LPC, Université Blaise Pascal, CNRS/IN2P3, Clermont, France*
[14] *LPSC, Université Joseph Fourier Grenoble 1, CNRS/IN2P3, Institut National Polytechnique de Grenoble, Grenoble, France*
[15] *CPPM, Aix-Marseille Université, CNRS/IN2P3, Marseille, France*
[16] *LAL, Université Paris-Sud, CNRS/IN2P3, Orsay, France*
[17] *LPNHE, Universités Paris VI and VII, CNRS/IN2P3, Paris, France*
[18] *CEA, Irfu, SPP, Saclay, France*
[19] *IPHC, Université de Strasbourg, CNRS/IN2P3, Strasbourg, France*
[20] *IPNL, Université Lyon 1, CNRS/IN2P3, Villeurbanne, France and Université de Lyon, Lyon, France*
[21] *III. Physikalisches Institut A, RWTH Aachen University, Aachen, Germany*
[22] *Physikalisches Institut, Universität Freiburg, Freiburg, Germany*
[23] *II. Physikalisches Institut, Georg-August-Universität Göttingen, Göttingen, Germany*
[24] *Institut für Physik, Universität Mainz, Mainz, Germany*
[25] *Ludwig-Maximilians-Universität München, München, Germany*
[26] *Fachbereich Physik, Bergische Universität Wuppertal, Wuppertal, Germany*
[27] *Panjab University, Chandigarh, India*
[28] *Delhi University, Delhi, India*
[29] *Tata Institute of Fundamental Research, Mumbai, India*
[30] *University College Dublin, Dublin, Ireland*
[31] *Korea Detector Laboratory, Korea University, Seoul, Korea*
[32] *CINVESTAV, Mexico City, Mexico*
[33] *FOM-Institute NIKHEF and University of Amsterdam/NIKHEF, Amsterdam, The Netherlands*
[34] *Radboud University Nijmegen/NIKHEF, Nijmegen, The Netherlands*
[35] *Joint Institute for Nuclear Research, Dubna, Russia*
[36] *Institute for Theoretical and Experimental Physics, Moscow, Russia*
[37] *Moscow State University, Moscow, Russia*
[38] *Institute for High Energy Physics, Protvino, Russia*
[39] *Petersburg Nuclear Physics Institute, St. Petersburg, Russia*
[40] *Stockholm University, Stockholm and Uppsala University, Uppsala, Sweden*
[41] *Lancaster University, Lancaster LA1 4YB, United Kingdom*
[42] *Imperial College London, London SW7 2AZ, United Kingdom*
[43] *The University of Manchester, Manchester M13 9PL, United Kingdom*
[44] *University of Arizona, Tucson, Arizona 85721, USA*

[45] University of California Riverside, Riverside, California 92521, USA
[46] Florida State University, Tallahassee, Florida 32306, USA
[47] Fermi National Accelerator Laboratory, Batavia, Illinois 60510, USA
[48] University of Illinois at Chicago, Chicago, Illinois 60607, USA
[49] Northern Illinois University, DeKalb, Illinois 60115, USA
[50] Northwestern University, Evanston, Illinois 60208, USA
[51] Indiana University, Bloomington, Indiana 47405, USA
[52] Purdue University Calumet, Hammond, Indiana 46323, USA
[53] University of Notre Dame, Notre Dame, Indiana 46556, USA
[54] Iowa State University, Ames, Iowa 50011, USA
[55] University of Kansas, Lawrence, Kansas 66045, USA
[56] Kansas State University, Manhattan, Kansas 66506, USA
[57] Louisiana Tech University, Ruston, Louisiana 71272, USA
[58] University of Maryland, College Park, Maryland 20742, USA
[59] Boston University, Boston, Massachusetts 02215, USA
[60] Northeastern University, Boston, Massachusetts 02115, USA
[61] University of Michigan, Ann Arbor, Michigan 48109, USA
[62] Michigan State University, East Lansing, Michigan 48824, USA
[63] University of Mississippi, University, Mississippi 38677, USA
[64] University of Nebraska, Lincoln, Nebraska 68588, USA
[65] Rutgers University, Piscataway, New Jersey 08855, USA
[66] Princeton University, Princeton, New Jersey 08544, USA
[67] State University of New York, Buffalo, New York 14260, USA
[68] Columbia University, New York, New York 10027, USA
[69] University of Rochester, Rochester, New York 14627, USA
[70] State University of New York, Stony Brook, New York 11794, USA
[71] Brookhaven National Laboratory, Upton, New York 11973, USA
[72] Langston University, Langston, Oklahoma 73050, USA
[73] University of Oklahoma, Norman, Oklahoma 73019, USA
[74] Oklahoma State University, Stillwater, Oklahoma 74078, USA
[75] Brown University, Providence, Rhode Island 02912, USA
[76] University of Texas, Arlington, Texas 76019, USA
[77] Southern Methodist University, Dallas, Texas 75275, USA
[78] Rice University, Houston, Texas 77005, USA
[79] University of Virginia, Charlottesville, Virginia 22901, USA
[80] University of Washington, Seattle, Washington 98195, USA

(Dated: June 3, 2010)

We present a new measurement of the $WZ \to \ell\nu\ell\ell$ ($\ell = e, \mu$) cross section and limits on anomalous triple gauge couplings. Using 4.1 fb^{-1} of integrated luminosity of $p\bar{p}$ collisions at $\sqrt{s} = 1.96$ TeV, we observe 34 WZ candidate events with an estimated background of 6.0 ± 0.4 events. We measure the WZ production cross section to be $3.90^{+1.06}_{-0.90}$ pb, in good agreement with the standard model prediction. We find no evidence for anomalous WWZ couplings and set 95% C.L. limits on the coupling parameters, $-0.075 < \lambda_Z < 0.093$ and $-0.027 < \Delta\kappa_Z < 0.080$, in the HISZ parameterization for a $\Lambda = 2$ TeV form factor scale. These are the best limits to date obtained from the direct measurement of the WWZ vertex.

PACS numbers: 12.60.Cn, 13.85.Qk, 14.70.Fm, 14.70.Hp

The standard model (SM) of particle physics has been extensively tested in the past three decades and is found to be in excellent agreement with experimental observations. It is widely assumed, however, that the SM is only a low energy approximation of a more general theory. Therefore, any significant deviation from the SM predictions yields information on the nature of a more fundamental theory. Production of WZ pairs is the least studied diboson process within the SM, as it is a charged final state and can only be produced at hadron colliders. A detailed study of this process probes the electroweak sector of the SM. In addition, searches for new phenomena in the production of heavy gauge boson pairs are interesting, as many extensions of the SM predict [1–4] additional heavy gauge bosons that can decay into a WZ boson pairs.

In the SM, WZ boson pairs are produced at leading order (LO) via t-, u-, and s-channels. These channels inter-

*with visitors from [a]Augustana College, Sioux Falls, SD, USA, [b]The University of Liverpool, Liverpool, UK, [c]SLAC, Menlo Park, CA, USA, [d]ICREA/IFAE, Barcelona, Spain, [e]Centro de Investigacion en Computacion - IPN, Mexico City, Mexico, [f]ECFM, Universidad Autonoma de Sinaloa, Culiacán, Mexico, and [g]Universität Bern, Bern, Switzerland.

fere and maintain unitarity at high energies. In the case of the t- and u-channels, the W and Z bosons are radiated from initial state quarks, while the s-channel production occurs via the WWZ triple gauge boson vertex, which is a consequence of the non-Abelian nature of the SM. There are 14 free parameters describing the generalized Lagrangian for the WWV interaction [5, 6], where V is either a Z boson or a photon. Assuming gauge invariance and conservation of the C, P, and CP symmetries, only six remain. Their notation and SM values are $\lambda_V = 0$, $\kappa_V = g_1^V = 1$ for the WWV vertex, while the deviations from the SM values are noted as $\Delta\kappa_V$, Δg_1^V, and λ_V. The $U(1)$ electromagnetic gauge invariance implies $\Delta g_1^\gamma = 0$. In this Letter, we describe the WWZ vertex in three-dimensional (3D) phase space of coupling parameters, $\Delta\kappa_Z$, Δg_1^Z, and λ_Z. We also consider the HISZ parameterization [7] that implies $\Delta\kappa_Z = \Delta g_1^Z(\cos^2\theta_W - \sin^2\theta_W)$. Thus, the WWZ vertex can be described by $\Delta\kappa_Z$ and λ_Z only.

If the coupling parameters have non-SM values, new physics is required to prevent gauge boson production from violating unitarity at high energies. The high energy behavior is controlled by introducing a dipole form factor scale, Λ, in the description of the couplings, $\alpha(\hat{s}) \to \alpha_0/(1+\hat{s}/\Lambda^2)^2$, where $\hat{s}$ is the square of the partonic center-of-mass energy and α_0 is the coupling value in the low energy approximation.

The WZ production cross section was previously measured to be $\sigma(p\bar{p} \to WZ) = 5.0^{+1.8}_{-1.6}$ pb [8] and $\sigma(p\bar{p} \to WZ) = 2.7^{+1.7}_{-1.3}$ pb [9], by the CDF and D0 collaborations, respectively, using $\sim$1 fb^{-1} of integrated luminosity. Combined limits on the gauge couplings from the CERN LEP collider were obtained [10] by the indirect measurement of the WWZ coupling in the $e^+e^- \to W^+W^-$ process. The only direct measurement of WWZ couplings was performed at the Tevatron. Using 1 fb^{-1} of integrated luminosity, 95% C.L. limits on anomalous WWZ couplings were derived [9] by the D0 experiment: $-0.17 < \lambda_Z < 0.21$, $-0.14 < \Delta g_1^Z < 0.34$ for the HISZ relation and $-0.12 < \Delta\kappa_Z = \Delta g_1^Z < 0.29$, using $\Lambda = 2$ TeV. The CDF experiment used data equivalent to 350 pb^{-1} of integrated luminosity that resulted in 95% C.L. limits on anomalous WWZ couplings [11]: $-0.28 < \lambda_Z < 0.28$ and $-0.50 < \Delta\kappa_Z < 0.43$ assuming equal coupling relation between WWZ and $WW\gamma$ couplings and $\Lambda = 1.5$ TeV.

In this Letter, we present a new measurement of the WZ production cross section and set 95% C.L. limits on the deviation from the SM predictions of triple gauge couplings (λ_Z, $\Delta\kappa_Z$, Δg_1^Z) using data equivalent to 4.1 fb^{-1} of integrated luminosity of $p\bar{p}$ collisions at $\sqrt{s} = 1.96$ TeV at the Tevatron collected by the D0 detector. This supersedes the previous D0 measurement. We consider only the leptonic decays of the W and Z bosons into final states with electrons, muons, and with missing transverse energy ($\not\!\!E_T$) [12] due to the neutrino from the W boson decay.

The detailed description of the D0 detector can be found elsewhere [13], while here we present a brief overview of the main sub-systems of the detector. The inner most part is a central tracking system surrounded by a 2 T superconducting solenoidal magnet. The two components of the central tracking system, a silicon microstrip tracker and a central fiber tracker, are used to reconstruct interaction vertexes and provide the measurement of the momentum of charged particles. The tracking system and a magnet are followed by the calorimetry system that consists of central (CC) and endcap (EC) electromagnetic and hadronic uranium-liquid argon sampling calorimeters, and an intercryostat detector (ICD). A central calorimeter and two endcap calorimeters cover the pseudorapidity ranges $|\eta| < 1.1$ and $1.5 < |\eta| < 4.2$, respectively, while the ICD provides coverage for $1.1 < |\eta| < 1.4$. The calorimeter measures energy of hadrons, electrons, and photons. Outside of the D0 calorimeter lies a muon system which consists of layers of drift tubes and scintillation counters and a 1.8 T toroidal magnet.

An electron candidate is identified as a cluster of energy in the CC, EC, or ICD that is matched to a track reconstructed in the D0 central tracker. Due to different coverage of the tracker, we select EC electrons within $1.5 < |\eta| < 2.5$ and CC electrons within $|\eta| < 1.1$. The cluster in the CC or EC must be isolated and have a shower shape consistent with that of an electron. In the intercryostat region (ICR), $1.1 < |\eta| < 1.5$, we cluster energy found in the CC, ICD, or EC detectors. These ICR electrons are required to pass a neural network discriminant that uses the cluster's shower shape and associated track information. A muon candidate is reconstructed as segments within the muon system that are matched to a track reconstructed in the central tracker. The muon candidate track must be isolated from activity in the tracker and the calorimeter.

The Monte Carlo (MC) samples of WZ signal and ZZ background are produced using the PYTHIA [14] generator. The production of the W and Z bosons in association with jets (W+jets, Z+jets), collectively referred to as V+jets, and $t\bar{t}$ processes are generated using ALPGEN [15] interfaced with PYTHIA for showering and hadronization. All MC samples are passed through the GEANT [16] simulation of the D0 detector. The simulated samples are further corrected to describe the luminosity dependence of the trigger and reconstruction efficiencies in data, as well as the beam spot position. All MC samples are normalized to the luminosity in data using next-to-leading order (NLO) calculations of the cross sections and are subject to the same selection criteria as that applied to data.

We consider four independent decay signatures: $eee + \not\!\!E_T$, $ee\mu + \not\!\!E_T$, $\mu\mu e + \not\!\!E_T$, and $\mu\mu\mu + \not\!\!E_T$. Electron reconstructed in the ICR must be selected as one of the electrons from the Z boson decay. We require the events to

Channel	$\mathcal{A} \times \epsilon$ (%)
eee	1.35 ± 0.15
$ee\mu$	1.57 ± 0.12
$\mu\mu e$	1.07 ± 0.11
$\mu\mu\mu$	1.34 ± 0.13

TABLE I: Acceptance multiplied by efficiency, $\mathcal{A} \times \epsilon$, of the full selection criteria for each decay signature. $\mathcal{A} \times \epsilon$ values are calculated with respect to the fully leptonic WZ decay simulation. The uncertainties are both statistical and systematic.

have at least three lepton candidates with $p_T > 15$ GeV that originate from the same vertex and separated from each other by at least $\Delta R = \sqrt{(\Delta\phi)^2 + (\Delta\eta)^2} > 0.5$. The event must also have a significant $\not\!\!E_T$ to account for the unobserved neutrino. We require $\not\!\!E_T$ to be above 20 GeV. Events are selected using triggers based on electrons and muons. Since there are multiple high p_T leptons from the decay of the heavy gauge bosons the trigger efficiency is measured to be $98\% \pm 2\%$ for all signatures.

In the WZ candidate selection, we first identify the leptons from the Z boson decay. We consider all pairs of electrons or muons, additionally requiring opposite electrical charge in the cases of muon pairs or electron pairs including an ICR electron. The pair that has an invariant mass closest to and consistent with the Z boson nominal mass is selected as coming from the Z boson decay. If such pair is not found the event is rejected. The lepton from the W boson decay is selected as the one with the highest transverse momentum from the remaining unassigned muons and CC or EC electrons in the event. This assignment is studied in the simulation and found to be 100% correct for $ee\mu$ and $\mu\mu e$ channels. It is found to be correct in about 92% and 89% of cases for eee and $\mu\mu\mu$ signatures, respectively. The effects of misassignment on the product of acceptance and efficiency of the selection criteria, $\mathcal{A} \times \epsilon$, are estimated in the signal simulation. Values of $\mathcal{A} \times \epsilon$ measured using the assignment method described above differ from those obtained using MC generator-level information by less than one per cent. Therefore, the systematic uncertainty on $\mathcal{A} \times \epsilon$ due to the misassignment is neglected in this analysis.

In order to reduce the background contamination, the thresholds in the selection criteria are further optimized for each WZ decay mode by maximizing $S/\sqrt{S+B}$. Here, S is the expected number of WZ signal events and B is the total number of background events. The simulation is used to estimate S as well as to measure $\mathcal{A} \times \epsilon$ for each decay signature. The kinematic selection criteria are applied to measure the acceptance in simulations, while the lepton identification efficiencies are measured in data. The results are summarized in Table I.

The major background is from processes with a Z boson and an additional object misidentified as the lepton from the W boson decay. Such processes are Z+jets, ZZ, and $Z\gamma$. A small background contribution is expected from processes without Z boson, such as W+jets and $t\bar{t}$ processes.

The ZZ and $t\bar{t}$ backgrounds are estimated from the simulation, while the V+jets, with V being either a Z or W bosons, and $Z\gamma$ backgrounds are estimated using data-driven methods.

One or more jets in the V+jets process can be misidentified as a lepton from the W or Z boson decays. To estimate this contribution, we define a *false* lepton category for electrons and muons. A *false* electron is required to have most of its energy deposited in the electromagnetic calorimeter and satisfy electron calorimeter isolation criteria, while having a shower shape inconsistent with that of an electron. A muon candidate is categorized as *false* if it fails the isolation criteria. These requirements ensure that the *false* lepton is either a misidentified jet or a lepton from the semi-leptonic decay of heavy flavor quarks. Using a multijet data sample, we measure the ratio of misidentified leptons passing two different selection criteria, *false* lepton and signal lepton, as a function of p_T and η for electrons and muons, respectively. We then select a sample of Z boson decays with an additional *false* lepton candidate for each final state signature. The contribution from the V+jets background is estimated by scaling the number of events in this sample by the corresponding p_T- or η-dependent misidentification ratio.

Initial or final state radiation in $Z\gamma$ events can mimic the signal process if the photon either converts into e^+e^- pair or when a central track is wrongly matched to a photon. As a result, the $Z\gamma$ process is a background to two out of the four final state signatures with $W \to e\nu$ decays. To estimate the contribution from this background, we measure the rate at which a photon is misidentified as an electron. This is estimated using a data sample of $Z \to \mu\mu$ events with a final state radiation photon, since it offers an almost background-free source of photons due to the invariant mass, $M(\mu\mu\gamma)$, constraint to the Z boson mass. The muon decay of the Z boson is chosen to avoid an ambiguity when assigning the electromagnetic shower to the final state photon candidate. The misidentification rate is measured as a function of the p_T of the electromagnetic shower. The $Z\gamma$ contribution is estimated by multiplying the p_T-dependent misidentification rate by the photon p_T distribution in the $Z\gamma$ NLO MC simulation [17].

The selection yields 34 WZ candidate events with an estimated 23.3 ± 1.5 signal, and 6.0 ± 0.6 background events. The number of observed candidate events as well as the expected numbers of signal and background events for each signature are summarized in Table II. The distribution of the invariant mass of the Z boson candidates is given in Fig. 1. The transverse mass of the W boson

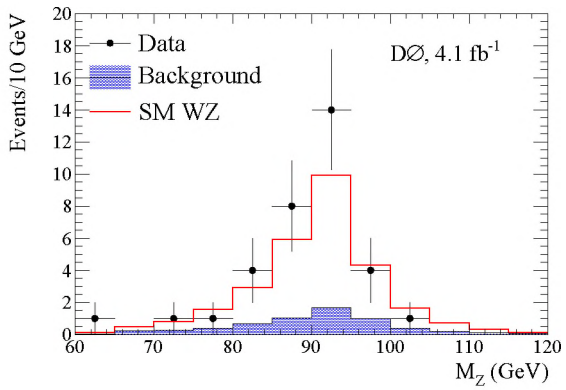

FIG. 1: (Color online) Invariant mass distribution of selected Z candidates in data (black points), with WZ signal (open histogram) and total background (dark histogram) overlaid.

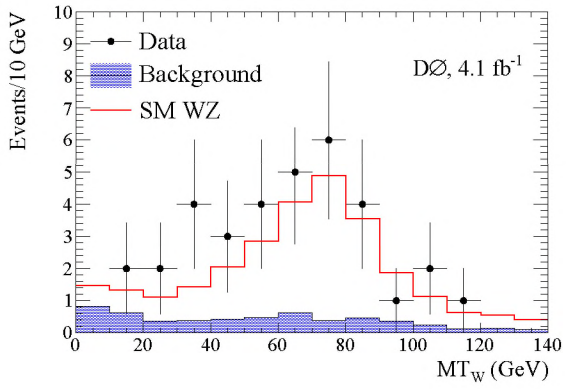

FIG. 2: (Color online) Transverse mass distribution of selected W candidates in data (black points), with WZ signal (open histogram) and total background (dark histogram) overlaid.

candidate is calculated as follows

$$MT_W = \sqrt{2E_T^\ell \not\!\!E_T (1 - \cos(\phi^\ell - \phi^{\not\!\!E_T}))}, \qquad (1)$$

where E_T^ℓ and ϕ^ℓ are transverse energy and azimuthal angle, respectively, of the electron or muon selected as the W boson decay product and $\phi^{\not\!\!E_T}$ is the azimuthal angle of the missing transverse momentum. The distribution of the W boson candidates is given in Fig. 2.

Several sources of systematic uncertainty are considered. The systematic uncertainties on the lepton identification efficiencies are 5%, 4%, and 6% for CC/EC electrons, muons, and ICR electrons, respectively. The systematic uncertainty assigned to the PDF choice is 5%. A systematic uncertainty of 5% is assigned on $\mathcal{A} \times \epsilon$ due to modeling of the kinematics of the WZ system. In addition, we assign 7% [18] and 10% [19] systematic uncertainty to the estimated $t\bar{t}$ and ZZ backgrounds, respectively, due to the uncertainty on their theoretical cross sections. The major sources of systematic uncertainty on the estimated V+jets contribution are the $\not\!\!E_T$ requirement and the statistics in the multijet sample used to measure the lepton misidentification ratios. These effects are estimated independently for each signature and found to be between 20-30%. The systematic uncertainty on the $Z\gamma$ background is estimated to be 40% and 58% for the eee and $\mu\mu e$ channels, respectively.

A likelihood method [20] is used to combine the four measurements, taking into account the correlations among the systematic uncertainties on the expected signal and the estimated background contributions. The cross section is $\sigma(WZ) = 3.90^{+1.01}_{-0.85}$ (stat + syst) $\pm$ 0.31 (lumi) pb. The uncertainties are dominated by the statistics of the number of observed candidates. The luminosity uncertainty includes 6.1% relative uncertainty [21] due to the luminosity measurement and the normalization uncertainty of the background contributions estimated from MC simulation.

The presence of anomalous WWZ couplings would lead to both an increase in the cross section and a change in the p_T spectrum of the W and Z bosons. We use the Z boson p_T distribution to set limits on the coupling parameters using a form factor scale $\Lambda = 2$ TeV. The Z boson p_T spectra from data, the SM, and two anomalous coupling predictions are shown in Fig. 3. The difference is most pronounced in the last bin, which includes also the events above 150 GeV.

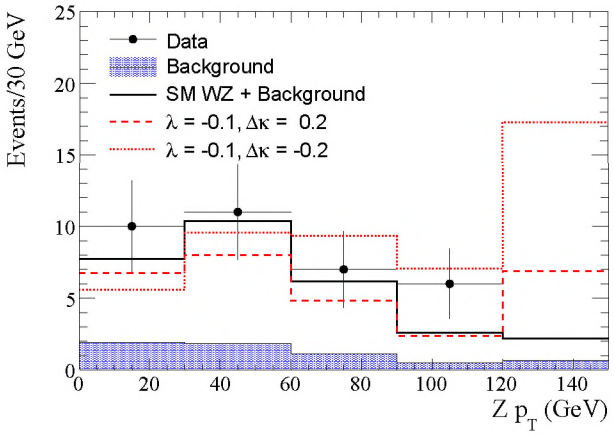

FIG. 3: (Color online) The Z boson p_T spectrum from data (points), total background (dark histogram), the SM WZ single + total background (open histogram), and two anomalous coupling models (dashed and dotted histograms). The last bin includes overflows.

A three-dimensional grid of values of anomalous couplings $\Delta\kappa_Z$, Δg_1^Z, and λ_Z is produced. For each point of the grid we generate WZ production using MCFM [19]

Source	eee	$ee\mu$	$e\mu\mu$	$\mu\mu\mu$
ZZ	0.39 ± 0.07	1.48 ± 0.20	0.40 ± 0.07	1.26 ± 0.23
V+jets	0.63 ± 0.17	0.56 ± 0.24	0.03 ± 0.01	0.17 ± 0.05
$Z\gamma$	0.28 ± 0.08	< 0.001	0.66 ± 0.34	< 0.001
$t\bar{t}$	0.03 ± 0.01	0.05 ± 0.01	0.04 ± 0.01	0.03 ± 0.01
Total bkg.	1.33 ± 0.21	2.11 ± 0.31	1.13 ± 0.35	1.46 ± 0.24
WZ signal	5.9 ± 0.8	6.9 ± 0.8	4.7 ± 0.6	5.8 ± 0.8
Observed	9	11	9	5

TABLE II: Number of observed events, expected number of signal events, and expected number of background events for each final state signature with total (statistical and systematic) uncertainties.

and obtain normalized to luminosity p_T spectrum of the Z boson. This spectrum combined with that from the estimated background is compared with the measured Z boson p_T spectrum in data. The likelihood of the match is calculated with the assumption of Poisson statistics for the signal and Gaussian uncertainties for the background. The two-dimensional 95% C.L. limit contours in three planes, $(\Delta\kappa_Z, \lambda_Z)$, $(\Delta g_1^Z, \lambda_Z)$, and $(\Delta g_1^Z, \Delta\kappa_Z)$, are shown in Fig. 4. In each case the third coupling is restricted to the SM value. For the HISZ parameterization the results are presented as limits on two coupling parameters: $\Delta\kappa_Z$ and λ_Z. The corresponding two-dimensional 95% C.L. limit contour is shown on Fig. 5. The one-dimensional limits on the coupling parameters obtained without any coupling relation and with HISZ parameterization are summarized in Table III.

Coupling relation	95% C.L. Limit
$\Delta g_1^Z = \Delta\kappa_Z = 0$	$-0.075 < \lambda_Z < 0.093$
$\lambda_Z = \Delta\kappa_Z = 0$	$-0.053 < \Delta g_1^Z < 0.156$
$\lambda_Z = \Delta g_1^Z = 0$	$-0.376 < \Delta\kappa_Z < 0.686$
$\Delta\kappa_Z = 0$ (HISZ)	$-0.075 < \lambda_Z < 0.093$
$\lambda_Z = 0$ (HISZ)	$-0.027 < \Delta\kappa_Z < 0.080$

TABLE III: One-dimensional 95% C.L. limits on anomalous coupling parameters obtained from varying one of the couplings while fixing the remaining couplings to the SM values (top three results). The last two results correspond to one-dimensional 95% C.L. limits on anomalous coupling parameters for the HISZ parameterization. A form factor scale of $\Lambda = 2$ TeV is used.

In summary, we have presented a measurement of the WZ production cross section using 4.1 fb^{-1} of integrated luminosity of D0 data. We observe 34 events with 23.3 ± 1.5 expected signal events and 6.0 ± 0.6 estimated background events. We measure the WZ cross section to be $3.90^{+1.06}_{-0.90}$ pb, which is in agreement with the SM NLO prediction of 3.25 ± 0.19 pb [19]. This is the most precise measurement to date of the WZ cross section. We find no evidence for anomalous WWZ couplings and set 95% C.L. limits of $-0.075 < \lambda_Z < 0.093$

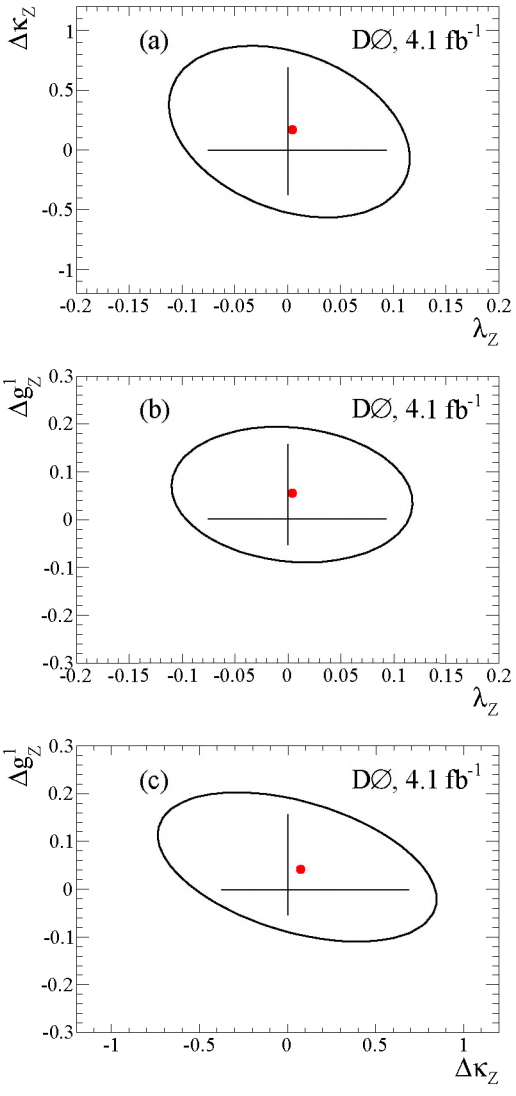

FIG. 4: (Color online) Two-dimensional 95% C.L limit contours on $(\Delta\kappa_Z, \lambda_Z)$ (a), $(\Delta g_1^Z, \lambda_Z)$ (b), and $(\Delta g_1^Z, \Delta\kappa_Z)$ (c). The point corresponds to the minimum of the likelihood surface. The vertical and horizontal lines represent the one-dimensional limits calculated separately. A form factor scale of 2 TeV is used.

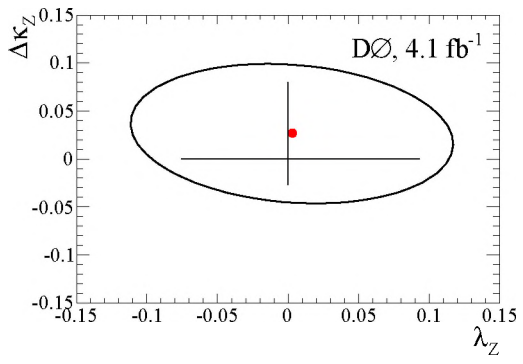

FIG. 5: (Color online) Two-dimensional 95% C.L limit contours for the HISZ parameterization. The point corresponds to the minimum of the likelihood surface. The vertical and horizontal lines represent the separately calculated one-dimensional limits.

and $-0.027 < \Delta\kappa_Z < 0.080$ for the HISZ parametrization using $\Lambda = 2$ TeV. These are the most stringent limits on WWZ couplings obtained from the study of direct WZ production.

We thank the staffs at Fermilab and collaborating institutions, and acknowledge support from the DOE and NSF (USA); CEA and CNRS/IN2P3 (France); FASI, Rosatom and RFBR (Russia); CNPq, FAPERJ, FAPESP and FUNDUNESP (Brazil); DAE and DST (India); Colciencias (Colombia); CONACyT (Mexico); KRF and KOSEF (Korea); CONICET and UBACyT (Argentina); FOM (The Netherlands); STFC and the Royal Society (United Kingdom); MSMT and GACR (Czech Republic); CRC Program and NSERC (Canada); BMBF and DFG (Germany); SFI (Ireland); The Swedish Research Council (Sweden); and CAS and CNSF (China).

[1] J.C. Pati, A. Salam, Phys. Rev. D **10**, 275 (1974) [Erratum ibid. D **11**, 703 (1975)]; R.N. Mohapatra, J.C. Pati, Phys. Rev. D **11**, 566 (1975); G. Senjanovic, R.N. Mohapatra, Phys. Rev. D **12**, 1502 (1975); G. Altarelli, B. Mele, M. Ruiz-Altaba, Z. Phys. C **45** (1989) 109 [Erratum ibid. C **47**, 676 (1990)].

[2] H. He *et al.*, Phys. Rev. D **78**, 031701 (2008); A. Belyaev, arXiv:0711.1919 [hep-ph] (2007); K.Agashe *et al.*, Phys. Rev. D **80**, 075007 (2009).

[3] M. Perelstein, Prog. Part. Nucl. Phys. **58**, 247 (2007).

[4] E. Eichten and K. Lane, Phys. Lett. B **669**, 235 (2008); K. Lane, Phys. Rev. D **60**, 075007 (1999).

[5] K. Hagiwara, R. D. Peccei, and D. Zeppenfeld, Phys. Rev. B **282**, 253 (1987).

[6] K. Hagiwara, J. Woodside, and D. Zeppenfeld, Phys. Rev. D **41**, 2113(1990).

[7] K. Hagiwara, S. Ishihara, R. Szalapski, and D. Zeppenfeld, Phys. Rev. D **48**, 2182 (1993); Phys. Lett. B **283**, 353 (1992).

[8] A. Abulencia *et al.*, CDF Collaboration, Phys. Rev. Lett. **98**, 161801 (2007).

[9] V. Abazov *et al.*, D0 Collaboration, Phys. Rev. D **76**, 111104 (2007).

[10] The LEP Collaborations ALEPH, DELPHI, L3, OPAL, http://lepewwg.web.cern.ch/LEPEWWG/lepww/tgc/summer03/gc_
.

[11] T. Aaltonen *et al.*, CDF Collaboration, Phys. Rev. D **76**, 111103 (2007).

[12] The D0 detector uses a right-handed coordinate system with the z axis pointing in the direction of the proton beam and the y axis pointing upwards. The azimuthal angle ϕ is defined in the xy plane measured from the x axis. The pseudorapidity is defined as $\eta = -\ln[\tan(\theta/2)]$, where $\theta = \arctan(\sqrt{x^2+y^2}/z)$. The transverse variable is defined as projection onto the $x-y$ plane. The missing transverse energy is the imbalance of the momentum estimated from the calorimeter cells and reconstructed muons in the $x-y$ plane.

[13] V.M. Abazov *et al.*, D0 Collaboration, Nucl. Instrum. Methods Phys. Res. A **565**, 463 (2006).

[14] T. Sjöstrand, S. Mrenna, and P. Skands, J. High Energy Phys. **05**, 026 (2006); we used V6.419.

[15] M. L. Mangano *et al.*, J. High Energy Phys. **07**, 1 (2003).

[16] GEANT Detector Description and Simulation Tool, CERN Program Library Long Writeup W5013.

[17] U. Baur and E. Berger, Phys. Rev. D **47**, 4889 (1993).

[18] P. M. Nadolsky *et al.*, Phys. Rev. D **78**, 013004 (2008).

[19] J. M. Campbell and R. K. Ellis, Phys. Rev. D **60**, 113006 (1999).

[20] G.J. Feldman and R.D. Cousins, Phys. Rev. D **57**, 3873 (1998).

[21] T. Andeen *et al.*, FERMILAB-TM-2365 (2007).